Bulletin of the Mineral Research and Exploration

http://bulletin.mta.gov.tr

Magnetic inversion modeling of subsurface geologic structures for mineral deposits mapping in southeastern Nigeria

Ema M. ABRAHAM[a*], Ayatu O. USMAN[a], Kelvin I. CHIMA[a], George-best AZUOKO[a] and Iheanyi IKEAZOTA[a]

[a] *Alex Ekwueme Federal University, Department of Geology/Geophysics, Ndufu-Alike Ikwo, P.M.B. 1010 Abakaliki, Ebonyi State, Nigeria*

Research Article

Keywords:
Magnetic modeling, Aeromagnetic data, Particle Swarm Optimization (PSO), Minerals, Depths.

ABSTRACT

Magnetic inversion techniques have been implemented to infer the extension and geometry of magnetic structures and also evaluate its influence on mineralization within Abakaliki and its environs, southeastern Nigeria. The modeling approach considers the techniques of three-dimensional (3D) magnetic data inversion, Euler deconvolution, analytic signal inversion, Enhanced Local Wavenumber (ELW) Technique and Particle Swarm Optimization (PSO) to estimate source parameters and compare results. Model solutions were interpreted to represent possible geologic units with varying trends, housing mineralization within the study region. Results from inversion computation over some active mine locations show subsurface bodies with magnetic susceptibilities >0.00188 SI. Model results also show structural sources with almost 5.5 km depth extension, stretching 18 km in the EW direction at Ngbo – Ekerigwe location. This could imply significant mineral deposits at the location. Inversion of both magnetic anomaly and analytical signal enabled derivation of the actual subsurface structures in the region, with most of the structures appearing as dykes with depths ranging from 0.2 – 1.8 km at most of the mining sites. Location and depths of some of the modeled intrusions have been corroborated with the active on-site mines. The delineation of mineralization structures by this study would guide systematic exploration in the region.

Received Date: 31.08.2022
Accepted Date: 30.03.2023

1. Introduction

Quantitative explanation of a potential field data includes assessment of depth, horizontal location, sources geometry as well as differences in the physical attributes (Essa and Abo-Ezz, 2021; Essa et al., 2021; Ganguli et al., 2021; Eshaghzadeh et al., 2020; Abraham and Alile, 2019; Essa et al., 2018; Aboud et al., 2018; Srivastava and Agarwal, 2010; Abdelrahman et al., 2003; Büyüksaraç et al., 1998, 2005). Modeling anomalies from a local magnetic field, and in particular, three - dimensional (3D) voxel-based modeling, is a contemporary and important tool in exploration targeting (MacLeod and Ellis, 2013). Inversion for a physical property involves the subdivision of the causative sources into a collection of rectangular cells, whose density or magnetization contrasts are to be appraised to explain the true distribution of the geological sources (Yao, 2007). 3D magnetic inversion allows total use of information in magnetic anomalies, estimating a 3D discrete physical property distribution that can describe the discerned geophysical field data (Li and Sun, 2016; Mahmoodi et al., 2016). In oil exploration, credible appraisals of depth to magnetic basement are

Citation Info: Abraham, E. M., Usman A. O., Chima K. I., Azuoko G., Ikeazota I. 2024. Magnetic inversion modeling of subsurface geologic structures for mineral deposits mapping in southeastern Nigeria. Bulletin of the Mineral Research and Exploration 173, 85-105. https://doi.org/10.19111/bulletinofmre.1267876

**Corresponding author: Ema M. ABRAHAM, ema.abraham@funai.edu.ng*

needed for improved comprehending of the crucial first-order basin examination parameters (Srivastava and Agarwal, 2010; Li, 2003). Magnetic inversion technique can resolve magnetic bodies possibly associated with zones having abundance of magnetite and other magnetic minerals, rendering structural knowledge regarding these magnetic bodies and in numerous occasions, about the structural system of the mineralization (Couto et al., 2017). 3D inversions have assisted interpretations just as magnetic data aids the characterization of ore bodies (Leâo-Santos et al., 2015; Büyüksaraç et al., 1998). On a regional scale, a cross-plot of density and susceptibility has been used (Melo et al., 2015; Kowalczyk et al., 2010) to define the classes of different lithologies and identify rock types. This approach can thus offer useful exploration information in areas with a paucity of geological information. Melo et al. (2015) used a comparable approach to demonstrate copper mineralization guided by the trend in the cross-plot of susceptibility and conductivity.

Various geophysical studies have been conducted around Abakaliki and environs. These include using Vertical Electrical Sounding (VES) technique to determine aquifer parameters, estimation of depth to magnetic source in a location closer to Abakaliki (Ugwu and Alasi, 2016), assessment of Curie Point Depth (CPD) (Abraham et al., 2018), hydrocarbon and mineral exploration prospect determination (Ezema et al., 2014) using aeromagnetic data and investigating the sequence of deposition of sedimentary strata in the region using seismic refraction and VES techniques (Agha and Arua, 2014). However, no three-dimensional (3D) inversion of magnetic data has been undertaken within the region towards the delineation of geological structures housing mineralization in the region. Inversion of magnetic survey data can offer restrictions on subsurface susceptibility allotments (Büyüksaraç et al., 2005; Lelievre, 2003). Abakaliki region is a mineralized province and has been documented to house great mineral potentials that include Lead, Zinc, Sodium Chloride, Silver, and Limestone (Abraham et al., 2018; Ugwu and Alasi, 2016; Ezema et al., 2014). This has been substantiated by mining activities (mostly local/small scale) ongoing in the region. Given the economic relevance of these minerals and the need to quantify the deposits for productive, extensive, and sustainable mining, the Nigerian government authorized an airborne magnetic and radiometric survey in the region betwixt 2005 and 2009. A close relationship exists between the proportion of magnetic minerals and magnetic susceptibility in rocks. Iron oxides; pyrrhotite, cobalt, nickel, and metallic iron are noteworthy. As these minerals, to the greatest extent, go with economic mineral deposits, we could analyze magnetic survey data to gain information on potential drilling targets (Lelievre, 2003). The creation of 2D and 3D models of geophysical inversion and mineral potential modeling has added to the large precompetitive data available to explorers (Büyüksaraç et al., 2005, 1998). The area of coverage by this study locates within geographic latitudes 6°00′ and 6°30′ *N* and geographic longitudes 8°00′ and 8°30′ *E* within the sedimentary terrain of southeastern Nigeria (Figure 1).

Our study seeks to carry out 2D and 3D magnetic inversion modeling, identify sources location, and perform depth analysis to geologic units bearing possible minerals in Abakaliki and environ. A credible depth appraisal to the top of causative source enhances budgeting as well as scheming of drill holes and other exploitation projects (Srivastava and Agarwal, 2010). We anticipate that the effect of this study will emphasize mineralized geologic units and structural positions and augments mining certainty in the region.

1.1. Geological Setting

Following a series of tectonic activities and recurrent sedimentation in the Cretaceous time, the Nigeria-Benue trough was formed. The split of the continents resulted in an abrupt rift (aulacogen) that has been stuffed with transgressive and regressive sedimentary lay downs (Ugwu and Alasi, 2016).

The lower Benue trough is supported below by a thick sedimentary succession set down in the Cretaceous era. Four geological formations which include the Nkporo Shale (Campanian), the Awgu Shale (Coniacian), the Asu River Group (Albian) and the Eze-Aku Shale (Turonian), constitutes the sediments that happened in the Abakaliki Anticlinorium (Figure 2). The sedimentary sequence was influenced by

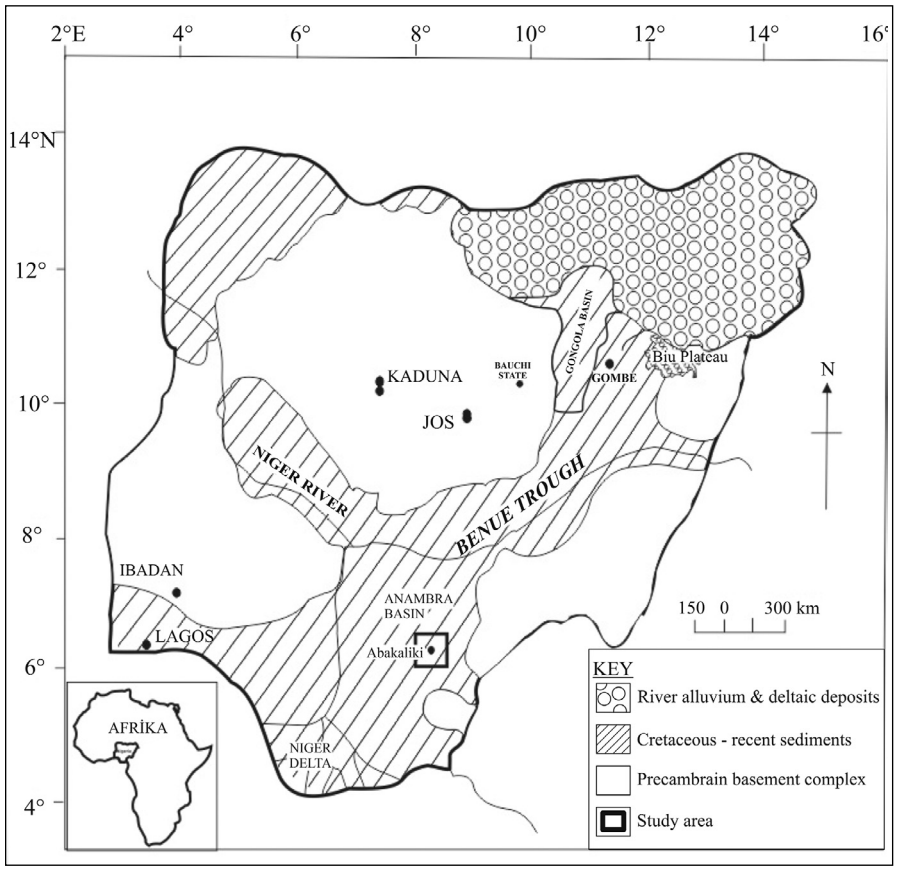

Figure 1- Map of Nigeria showing the general geology, location and coverage area of this study (modified from Abraham et al., 2018).

large-scale tectonic events that occur in two stages leading to folding of the sediments. Cenomanian and Santonian deformations affected the area with a large tectonic imprint (Nwachukwu, 1972; Olade, 1975; Ezema et al., 2014).

A general NE-SW trending fold characterized the Santonian deformation. The folding influenced the development of the Abakaliki Anticlinorium, a compressive structure marked with asymmetry and reversed faults. Benkhelil (1988) described the orogenic cycle of the anticlinorium to include sedimentation, magmatism, metamorphism, and compressive tectonism. Numerous intrusive bodies within the shale are due to magmatism that affected the Eze-Aku and Asu River Group (Figure 2). Majority of these intrusive has been concealed by the shale formation (general superficial geology) of the region as observed in the geology. This study offers supplemental information on the intrusive bodies including estimates of their respective depths. Intermediate intrusive appear on the surface and could be seen in parts of the study area like the Abakaliki town. This intrusive appears as sills (Ezema et al., 2014; Ofoegbu, 1985; Eze and Mamah, 1985). The Abakaliki shale (Asu River Group) is of Albian age, dark gray, blocky and non-micaceous in most locations. The Asu River Group is predominantly shale and localized incidences of sandstone, siltstone, and limestone intercalations. Eze-Aku formation comprises of a succession of calcareous sandstones.

Figure 3 shows the lithostratigraphic section (Obarezi and Nwosu, 2013) of the two main geologic units recognized in the study area. The lithostratigraphic section was erected from acquired and logged geologic core data. The interpreted data shows the trend and structure that controls mineralization, mineralogy, and the sequence of deformation. Figure 4 displays images of the current open cast mining of lead-zinc (Pb-Zn) minerals by the locals within the study region. Current mining operations at these regions are largely done by

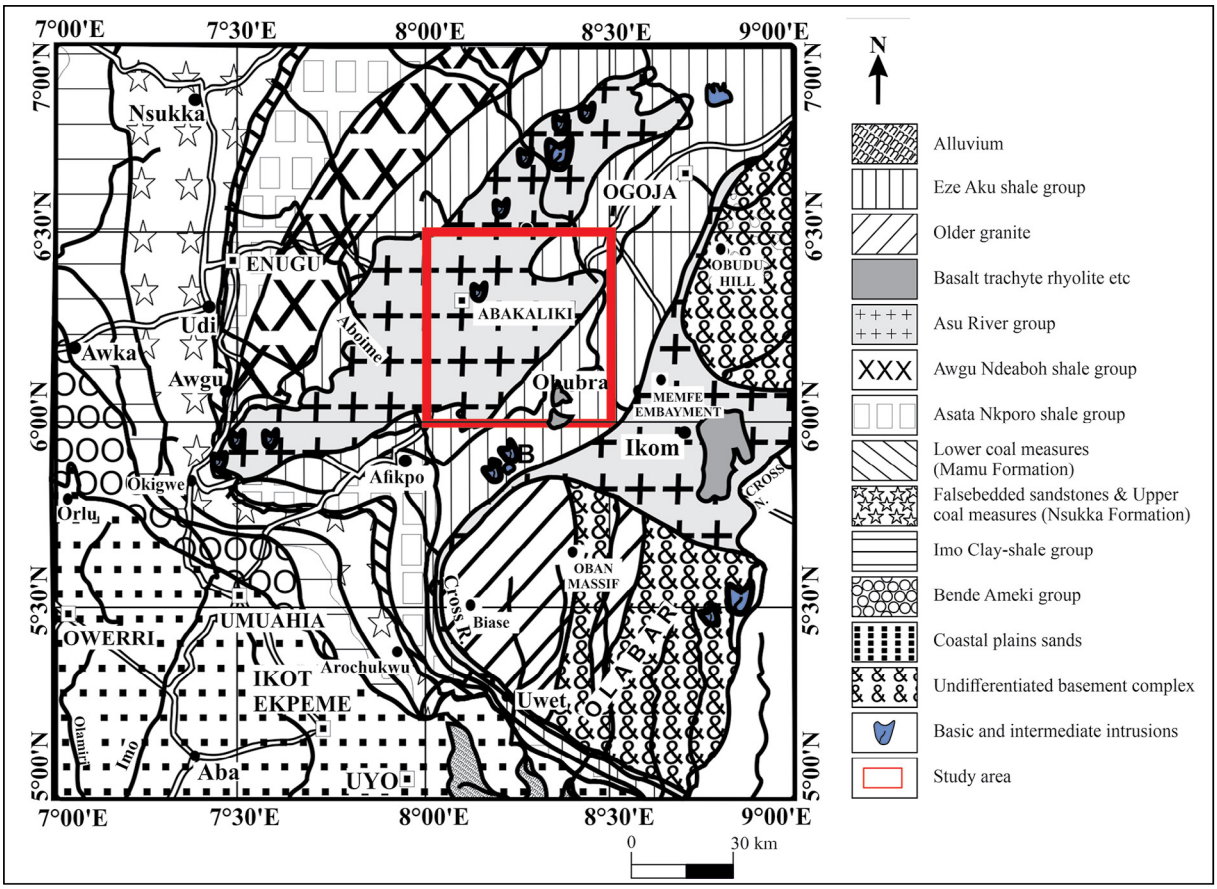

Figure 2- Detail geological map of southeastern Nigeria depicting the study area. The inserted red square represents the study area coverage in Figure 1 (modified from Abraham et al., 2018).

locals with crude tools and haphazard exploitation. Most of the mining is not mechanized as crude tools and poor excavation methods are employed by the locals to exploit these minerals. The water accumulations in some of the mines are mine water and rain accumulations.

2. Methods

Our study area is covered by a high-resolution digital aeromagnetic map sheet number 303 – Abakaliki, (Figure 5) spanning an area of approximately 3025 km^2. The airborne data was acquired for the Nigerian Geological Survey Agency (NGSA) in 2005 and 2009. The entire data include approximately 2 km line of magnetic as well as radiometric surveys carried out at 500 m line spacing using 80 m terrain clearance. The regional field and diurnal magnetic effects were removed from the data. We applied the Reduction to Equator (RTE) correction (Leu, 1981; Jain, 1988; Abraham et al., 2018; Ganguli et al., 2021) assuming a magnetic declination of -2.15° and an inclination of -13.91° for the study area utilizing the fast Fourier transform operator. Strong variations in magnetic intensities, suggesting different magnetic properties, could be discerned from the map.

Positive anomalies with higher values (90 – 94 nT) are observed at Onyen, Obubra, Ngbo, Abba Omega, and part of Enyigba localities. The positive anomalies at Obubra and Oyen regions may be due to intrusions of basalt, trachyte, Rhyolite and other intrusions within the region. This region locates within the Eze Aku Shale Group, largely notable for higher magnetic anomaly values (70 – 110 nT) (Figure 6). We note lower magnetic values around FUNAI, Ezzagu, and Egudenago localities between 19 nT and 40 nT. Within the Enyigba – FUNAI region, the notable lower magnetic anomaly unit observed, falls within the Asu River Group (Figure 6) and may be due to an intrusion within the Asu River shale formation. This

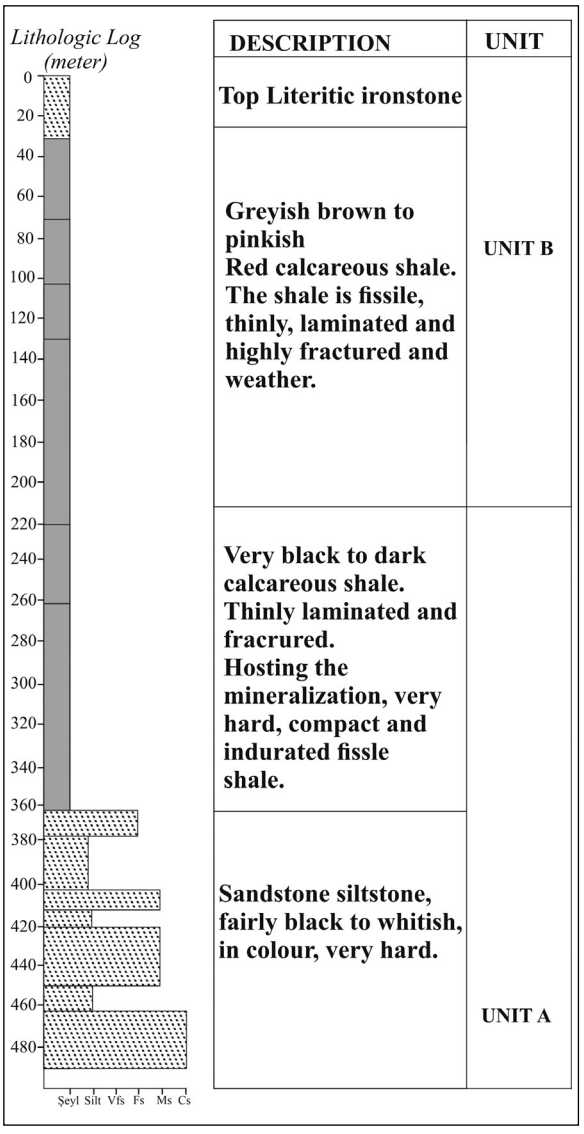

Figure 3- Lithostratigraphic section of the geologic units in the study area (modified from Obarezi and Nwosu, 2013)

(a) Ameri Mine (8.067°*E*, 6.300°*N*)

(b) Enyigba Mine (8.106°*E*, 6.174°*N*)

(c) Ameka Mine (8.100°*E*, 6.150°*N*)

(d) Mbaraekke Mine (8.270°*E*, 6.490°*N*)

Figure 4- Images of some of the mines location in which current mining of lead-zinc minerals is ongoing by the locals (as could be seen in the pictures).

may be true given the current exploitation of some mineral deposits from the region. A conspicuous E-W trending lower magnetic anomaly streak observed at northern region may be due to a lower magnetic susceptibility sill-like deposition located deeply in this region. The variation of magnetic strength (Total Field values) across the study area indicates the difference in susceptibility of the geological bodies, including mineralization and structures.

2.1. Magnetic Inversion

We present a brief theoretical insight into our adopted method for the 3D inversion. Pilkington (2009) used the Cauchy norm (Sacchi and Ulrych, 1995) to solve the 3D magnetic inverse problem for sparse models, i.e. those models in which the number of nonzero values that fit the data is minimized. The derived inversion is therefore regarded as geologically unconstrained, in comparison with constrained inversions in which hard geologic constraints like

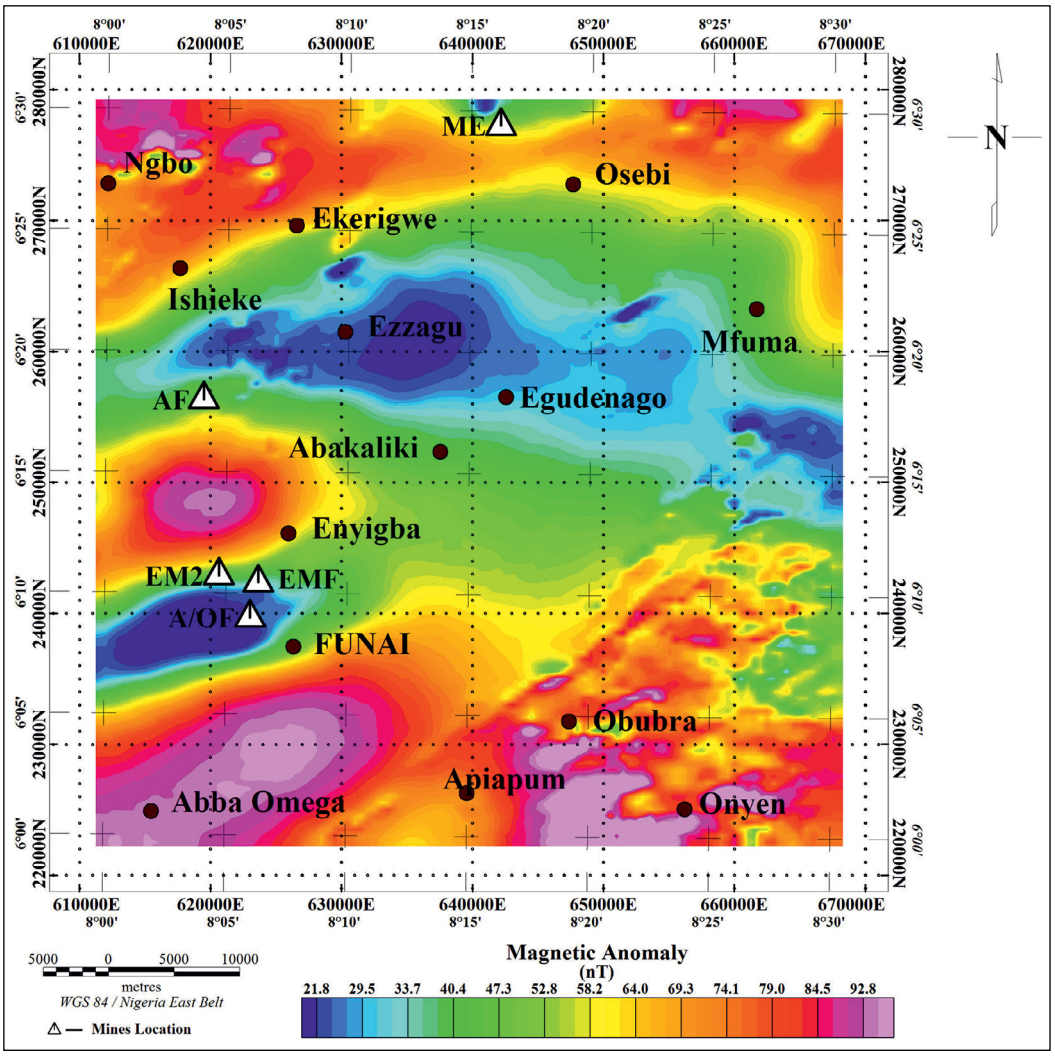

Figure 5- Aeromagnetic Anomaly map covering the region of study. Current and active mines (white triangles) are located on the map which includes the Ameri Mine Field (AF), Enyigba Mine Field (EMF), Ameka/Ohankwu Field (A/OF), Mkpuma-Ekwaokuko Field (ME) and Enyigba Mine Field 2 (EM2).

for example drill hole intersections are included (Pilkington, 2009).

For our computations, we assumed that all sources are magnetized by induction, having a susceptibility range starting from 0.0001 SI, an inclination of –13°, and declination –2°. We inverted the entire dataset to produce a 3D voxel susceptibility model using Pilkington and Bardossy (2015) implementation in the GEOSOFT program.

2.2. 3D Euler Deconvolution

Among the goals for performing the 3D Euler, the process includes outputting a map that exposes the depths of the geologic sources perceived in a 2D grid and their corresponding locations (Eshaghzadeh et al., 2020; Whitehead and Musselman, 2005). The standard 3D Euler technique is founded on Euler's homogeneity equation – an equation relating the magnetic or gravity field along with its gradient constituents to source position, with structural index, SI (the degree of homogeneity N) (Thompson, 1982). An exponential factor analogous to the ratio by which the potential field falls off with distance when a source with a given geometry is taken into account. For our computations, we adopted the standard 3D design of Euler's equation (Reid et al., 1990) as implemented by GEOSOFT Oasis Montaj software as:

$$x\frac{\partial T}{\partial x}+y\frac{\partial T}{\partial x}+z\frac{\partial T}{\partial x}+\eta T=x_o\frac{\partial T}{\partial x}+y_o\frac{\partial T}{\partial x}+z_o\frac{\partial T}{\partial x}+\eta b \quad (1)$$

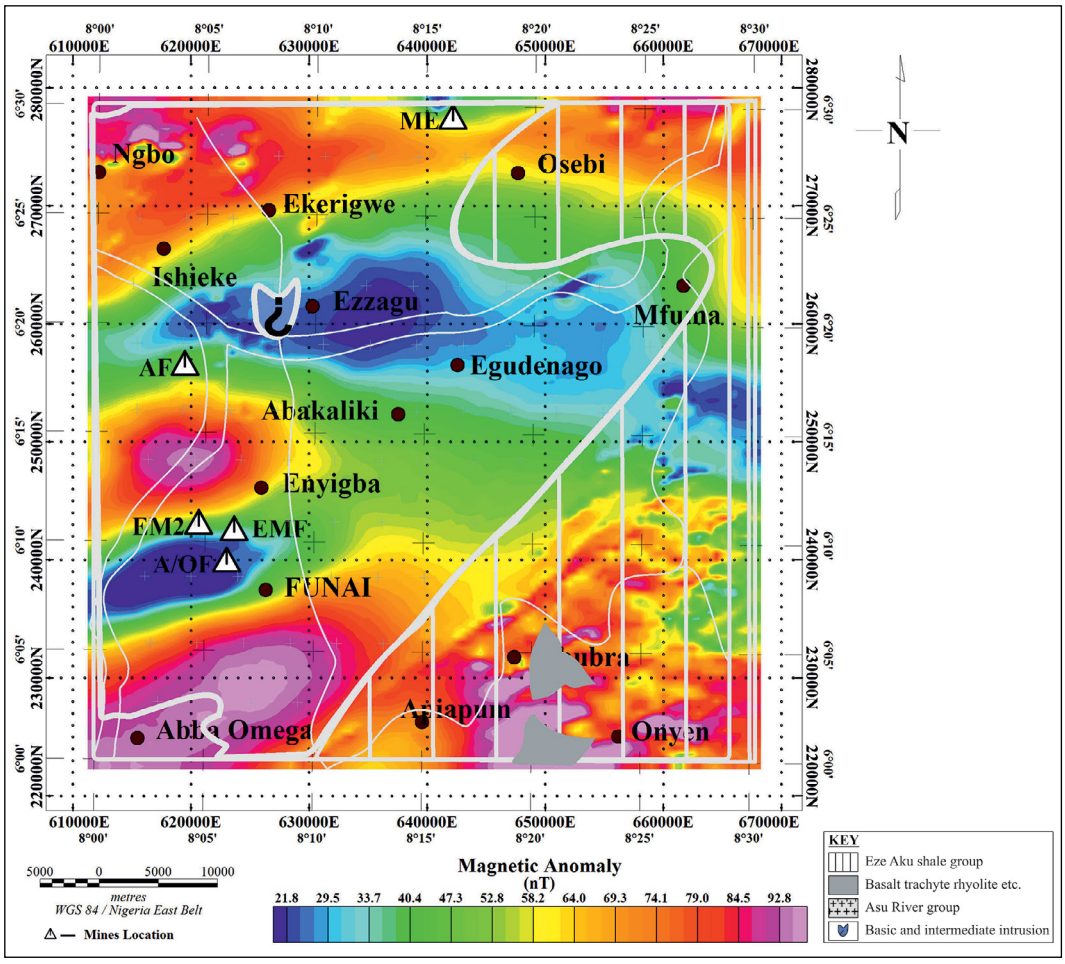

Figure 6- Aeromagnetic anomaly map with superimposed geology map of the study area.

where *x, y* and *z* represents coordinates of a measuring point, x_o, y_o and z_o represents coordinates of the source position of which the total field is discerned at *x, y* and *z*, *b* represent a base level, η represent the structural index (SI) and *T*, Total magnetic field. The source body type of interest determines the value of SI (Whitehead and Musselman, 2005). As an example (Kumar et al., 2020; Ganguli et al., 2019; Abraham and Alile, 2019; Thompson, 1982; Reid et al., 1990) proposes $\eta = 0$ for a contact, $\eta = 1$ (vertical dyke or the edge of a sill), $\eta = 2$ (centre of a horizontal or vertical cylinder), and $\eta = 3$ (centre of a magnetic orb or dipole). Euler's equation for magnetic data possesses a significant advantage because it is indifferent to magnetic inclination, declination, and remanence which constitute a constant, in the anomaly function of any given model. As we are interested in locating source contact/faults with depths, to model geological units influencing mineralization in Abakaliki and environs, we adopted an SI of 0 (Reid and Thurston, 2014) and a window size >=10 at 15% depth tolerance, for our computations.

2.3. Enhanced Local Wavenumber (ELW) Technique

Following the concept of local phase 2-D analytic signal of any constituents of the Earth's magnetic field assessments, an equation (autonomous of the causative source geometries) was obtained by Thurston and Smith (Thurston and Smith, 1997) utilizing second-order vertical and horizontal derivatives of magnetic anomalies. This includes the contact, thin sheet, pole and dipole, involving unknown parameters of location and depth only. Having known the horizontal position as well as depth parameters, the source geometry was further determined (Srivastava and Agarwal, 2010). For this study, we utilized a FORTRAN code developed by Agarwal and Srivastava (2008) to analyze field anomalies.

2.4. 3D Analytic Signal

Horizontal displacement regarding sources has always complicated the elucidation of observed magnetic anomalies. The non-vertical direction of the induced magnetization and geomagnetic field, results in displacement or skewness. To verify if the magnetic anomalies in the area were brought about by intrusions, we calculated the analytic signal response of the geomagnetic field. The 3D Analytic Signal amplitude is shown as (Roest et al., 1992; Riedel, 2008):

$$A(x,y) = \sqrt{\left(\frac{\partial T}{\partial x}\right)^2 + \left(\frac{\partial T}{\partial y}\right)^2 + \left(\frac{\partial T}{\partial z}\right)^2} \quad (2)$$

where T represents the observed field at x and y.

Despite this function not being a measurable parameter, it is highly fascinating in the context of interpretation, as it retains its independence in terms of the direction of magnetization, as well as the direction of the inducing field. This implies that all bodies with the same geometry have the same analytic signal. Maxima are displayed over magnetization contrasts and are independent of the ambient magnetic field including sources magnetization directions. These maxima thus outline the magnetic sources from their locations. The analytic signal is useful in identifying the edges of the magnetic source bodies, where remanence and/or low magnetic latitude (as in this study) makes interpretation difficult (Whitehead and Musselman, 2005).

2.5. Particle Swarm Optimization (PSO) and 2D Analytic Signal

To model the subsurface structure from the analytical signal and magnetic anomalies, we adopted the particle swarm optimization (PSO) technique. PSO results appear to be stable to a greater degree than other optimization techniques (Essa and Elhussein, 2020; Essa and Munschy, 2019; Srivastava and Agarwal, 2010). PSO (Srivastava et al., 2020; Srivardhan et al., 2016; Kennedy and Eberhart, 1995) is a global optimization method and is one of the accepted naturally influenced metaheuristic algorithms founded on the conduct of bird flocks as well as fish schools looking for food (Pallero et al., 2015). The purpose of a geophysical inverse problem is to discover a best reasonable model explaining a collection of observed data like an M-dimensional optimization problem (Srivastava and Agarwal, 2010). Following Srivastava and Agarwal (2010), we take into account the mapping, g betwixt the 'model space vector', **m** together with the 'data space vector', **d** as

$$d = g(m), \quad (3)$$

Also, take into account that the model m_{true} produces the observed data, d_{obs}:

$$d_{obs} = g(m_{true}) \quad (4)$$

The objective function is defined as

$$E(m) = [d_{obs} - g(m)]^T [d_{obs} - g(m)], \quad (5)$$

The superscript T represents the matrix transpose. When the appraised model **m** comes near to the true model, m_{true}, the objective function E(**m**) tends to minimum.

For the PSO, a swarm of particles is chosen by chance from the M-dimensional model space vector in order that the position of each particle matches to a could be model. A particle i possesses the next attributes at the kth iteration (flight): (1) current location, m_i^k (2) the best location accomplished so far m_i^n and (3) velocity, V_i^k. A velocity adaptation of the particle is resolved together by the previous best position filled by the particle as well as the best position of the swarm for each of the iterations. Computation of a new position on account of the particle is performed utilizing the new velocity. The part of the velocity adaptation resolved by the individual's previous best position is known as the 'cognition', and the part impacted by the best in the population is known as the 'social' part. The swarm, from the other point of view, possess but one characteristic, particularly, the best locations m_i^g , obtained up to the kth iteration. The cognitive and social knowledge determines the direction of each particle in the swarm. In mathematical form, this is described as (Srivastava and Agarwal, 2010):

$$m_i^{k+1} = m_i^k + a\left[V_i^k + b\, ran(.)\left(m_i^n - m_i^k\right) + c\, ran(.)\left(m_i^g - m_i^k\right)\right] \quad (6)$$

Parameters b and c stands for the learning rates controlling the cognition as well as the social knowledge, correspondingly. The parameter a

represents the constriction factor established by (Clerc, 1999) and is nearly connected to the inertia factor while ran(.) represents a random number generator (Press et al., 1994) picked in a uniform manner in the open interval (0, 1).

The amplitude of the Analytic Signal over a 2D source (AS) is a symmetrical function with peak almost agreeing with the upper corners of the causative source (Mehanee et al., 2021; Nabighian, 1972). Some researchers (Salem et al., 2005; Srivastava and Agarwal, 2010) demonstrated that AS of distinctive source geometries is capable of being approximated by a generalized equation following the form:

$$|A(x)| = \frac{K}{[(x - x_0)^2 + z_0^2]^q} \quad (7)$$

The amplitude factor, K, is connected to the physical characteristics of the source. The horizontal location and depth of the source is represented as x_0 and z_0, correspondingly, and the shape factor is represented as q. Equation (7) attains a maximum at $x = x_0$. PSO was used to invert AS to resolve horizontal location and depth, amplitude factor (K) and shape factor (q) for every corner of the adopted model. These parameters are determined by designating search spaces for constant K, shape factor q, as well as the horizontal location and depth (in connection with data spacing). The amplitude of analytic signal AS of a 2D magnetic source model as approached by an m-sided polygon is the sum of the m symmetric bell-shaped functions (equation 7) nearly centered atop corners of a polygon (Srivastava and Agarwal, 2010; Huang and Guan, 1998).

For the PSO implementation, we performed 10 independent runs utilizing 100 particles to achieve the optimum model parameters. Values 1, 2, and 2 were allocated for the inertia factor (a) as well as the cognitive and social scaling factors (b and c), correspondingly (Thompson, 1982). The variation in shape factor from 0.2 – 1.5 was considered to incorporate various types of source geometries. Results obtained from PSO were compared with those from ELW technique (Agarwal and Srivastava, 2008).

We computed a synthetic magnetic field data using a MATLAB program (Stocco et al., 2009). The code of the inversion routine is established on a weighted-damped least-squares algorithm, following a standard of balancing the weight of the data inaccuracies as well as the compactness of the solution.

3. Results

The best 3D susceptibility model was achieved at the 230th iteration on the magnetic anomalies with a root-mean-square (rms) error of 1.129485 nT and results displayed in Figure 7. Figure 8 displays the model result after clipping susceptibilities lower than 0.00113 SI. Figure 9 displays model result with superimposed magnetic data respectively.

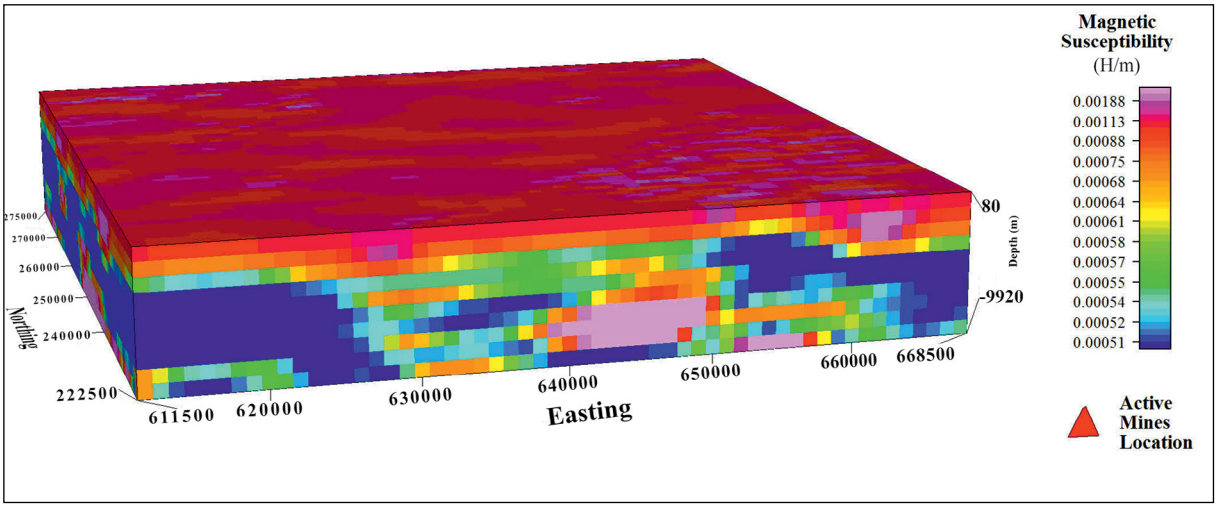

Figure 7- 3D model results from the inversion of magnetic data. The conspicuous contrast between the intruding structures and the host environment could be seen in the model with susceptibilities ≥0,00113 *SI.*.

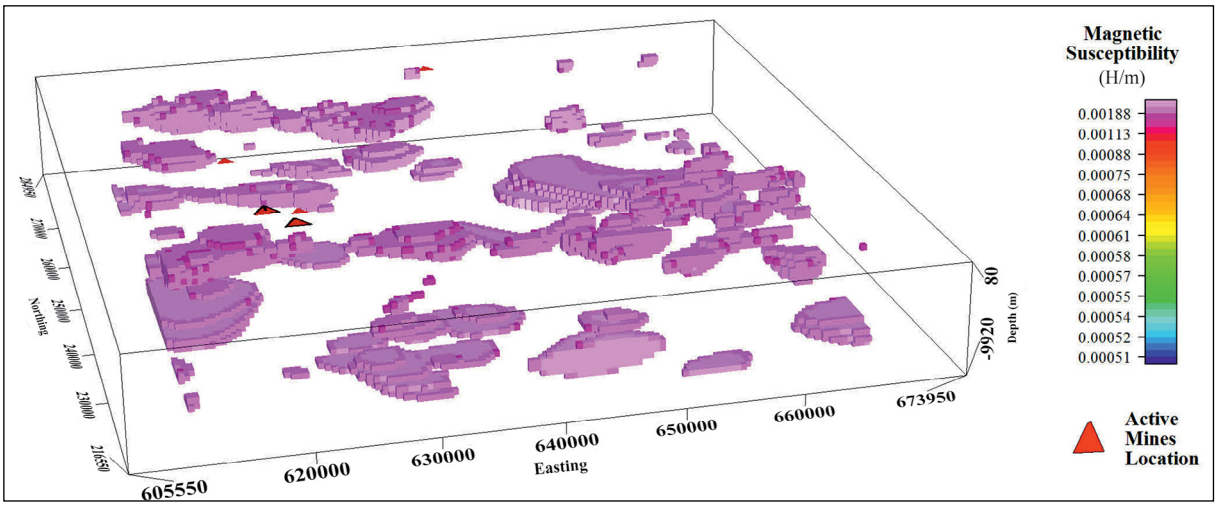

Figure 8- Model results after clipping susceptibilities lower than 0.00113 SI (Figure 7). A depth slice at -100 m was taken and the inversion model was constrained using information from Figure 2 (Geology) and 3 (Lithostratigraphic section) of Enyigba, in addition to Dobrin and Savit (1988).

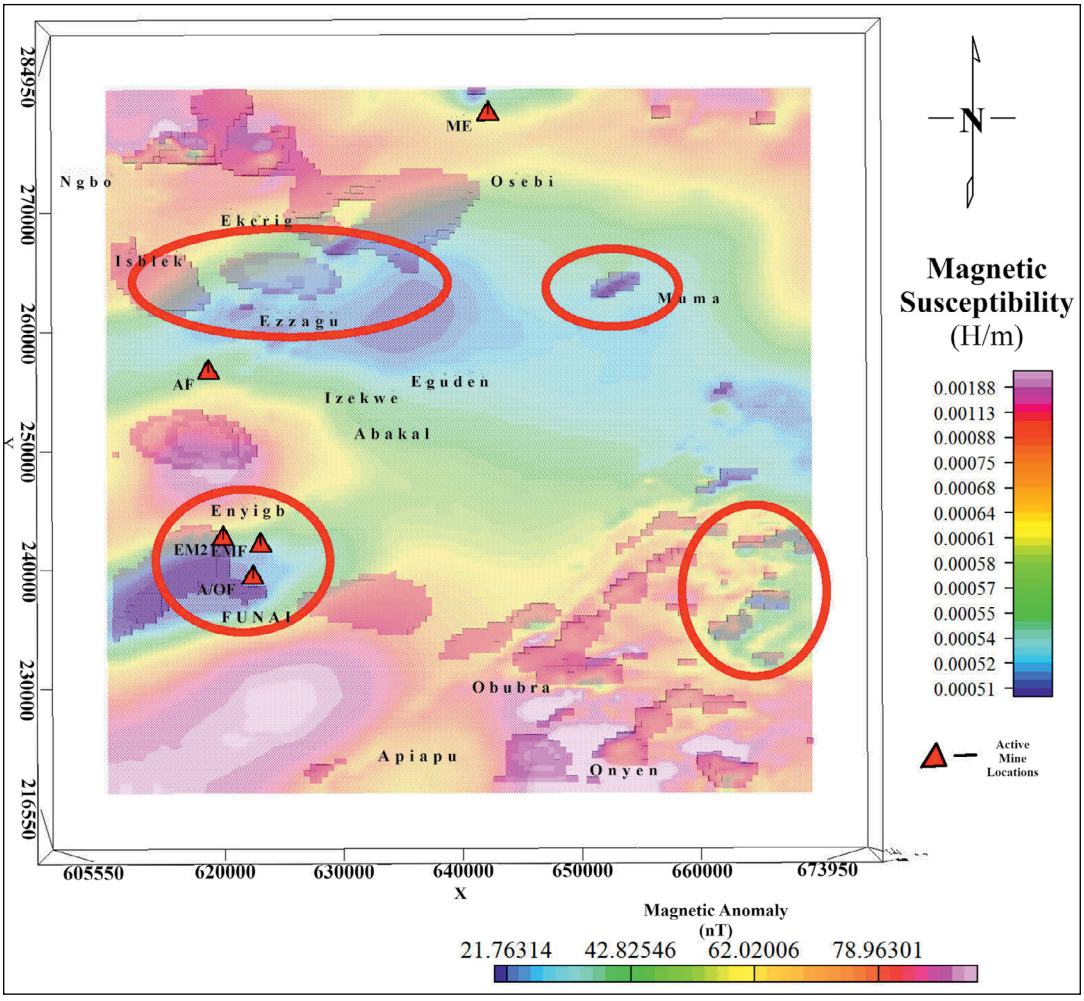

Figure 9- Plan view of the magnetic field anomaly (watermarked at 59% transparency) superimposed on the outlines of the model bodies. We noticed that some largely lower magnetic anomalies locate over high susceptibility units in the model (circled).

Results from 3D Euler deconvolution is presented in Figure 10 The presented result is a map showing Euler depth solutions superimposed on combined 3D susceptibility solutions (Plan view) map and magnetic anomaly data (with 59% transparency effect to enable see-through to some of the susceptibility solutions in the background).

The effect of the structural trends of possible subsurface geologic contacts mapped with the Euler deconvolution could be seen on the distribution of the model solutions from the inversion results (Figure 10). Parallel geologic structures trending NE –SW directions (inserted white lines), which may be faults structures 'sandwich' the mines clusters at Enyigba – FUNAI enclave and appears to control the existence of the mineral deposits in the region. A similar structural network is also noticed at the Ameri Mine Field (AF), above the Enyigba town. These are observed on individual examination of the Plan View display of model solutions. Figure 11 shows a map of the Analytic Signal computation. The profiles on the map possesses various parameters as summarized in Table 1.

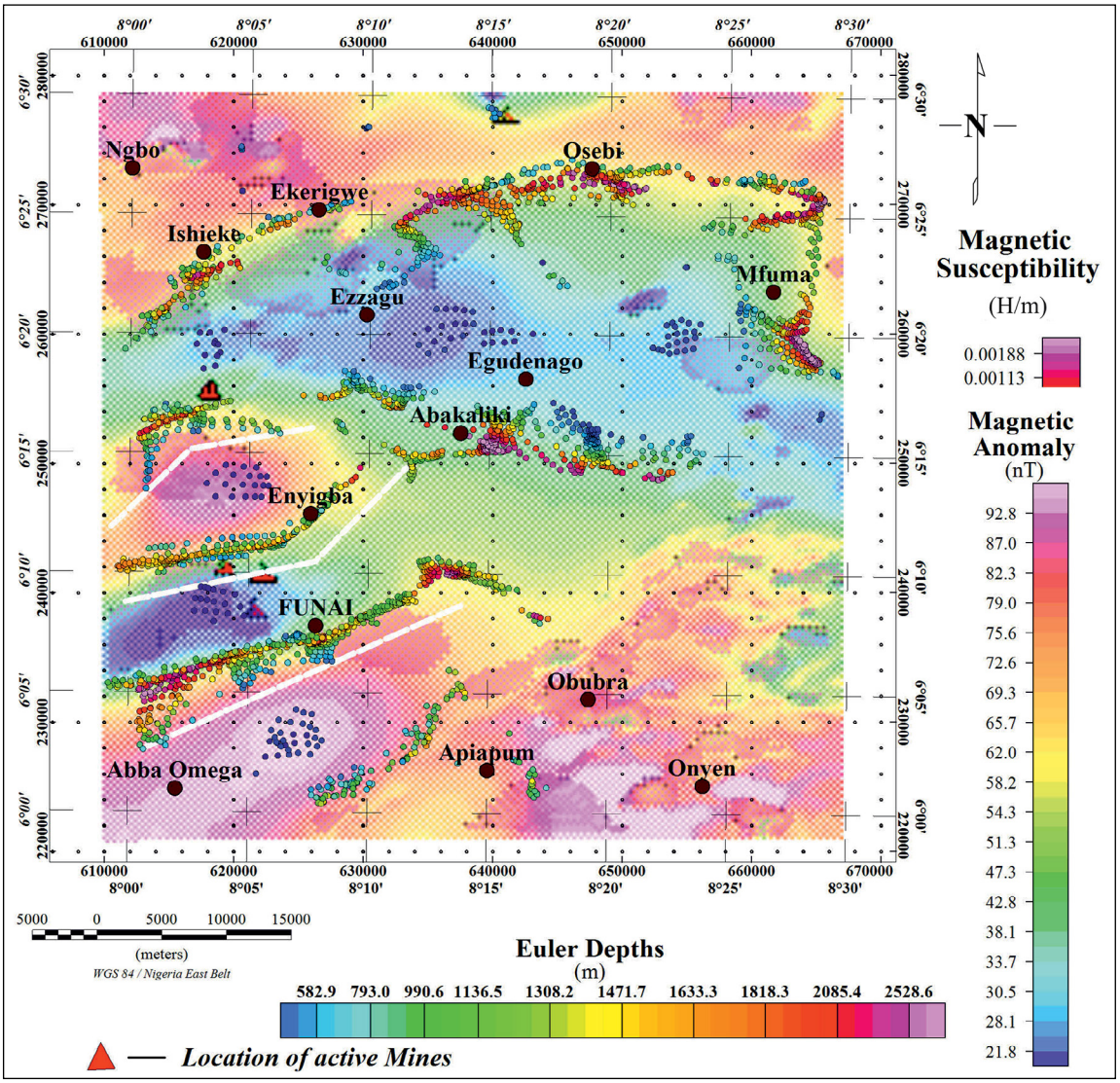

Figure 10- 3D Euler depths solutions overlain on the magnetic anomaly data (at 59% transparency) and 3D susceptibility model solutions.

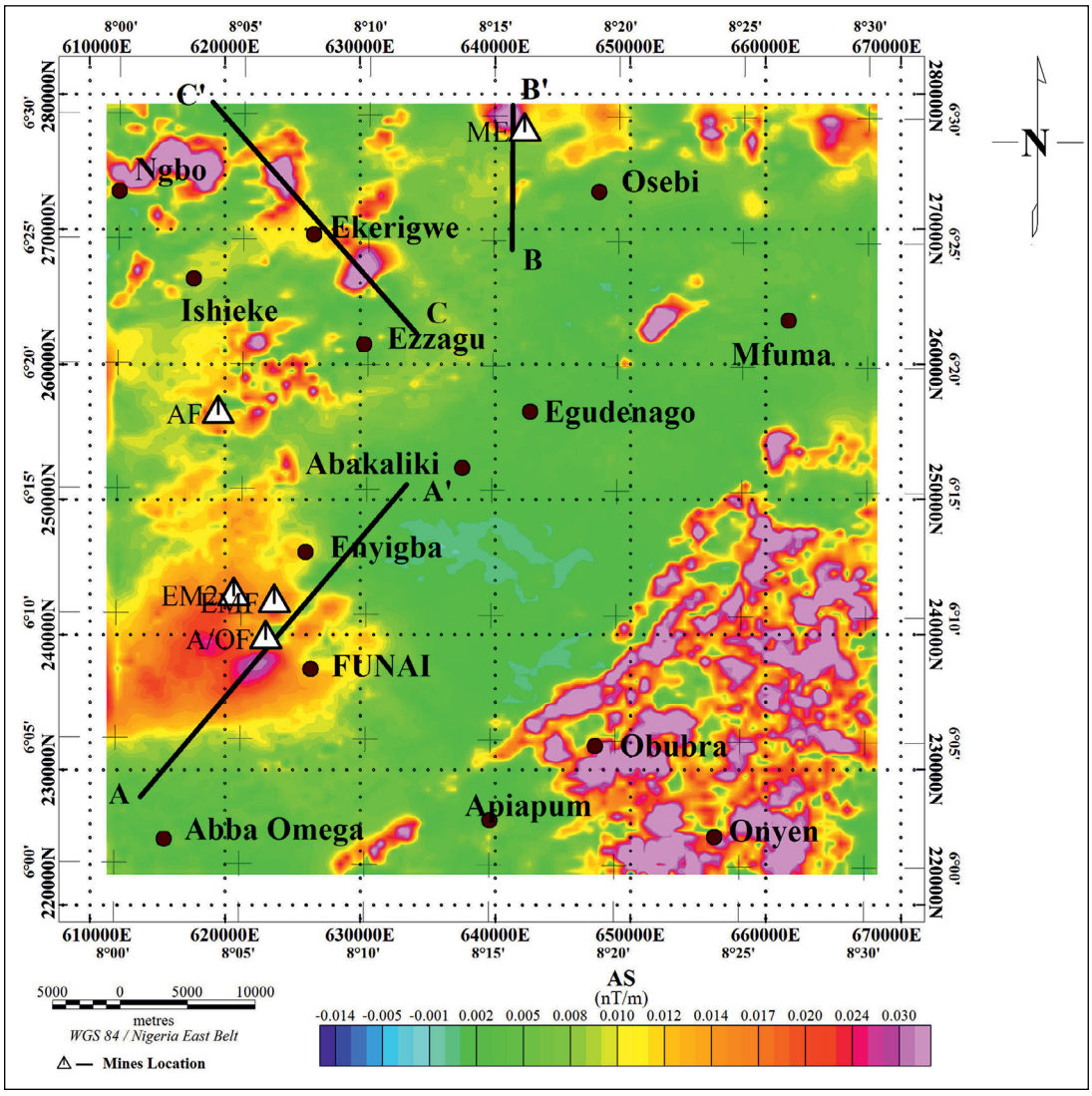

Figure 11- Analytic signal results of the study area. Various maxima observed on the map captures sources with strong magnetization contrast and provide information on their respective locations. Profiles *AA′*, *BB′* and *CC′* are taken on suspected anomalies especially at current mining sites. These were inverted and analyze to derive the actual subsurface structures at these sites

Table 1- Profile parameters to include longitude, latitude, length and azimuth.

	Longitude (°)	**Latitude** (°)	**Length (km)**	**Azimuth** (°)
Profile AA′	8.02 8.19	6.04 6.26	104.60	49.81
Profile BB′	8.26 8.26	6.41 6.51	103.38	90.00
Profile CC′	8.20 8.06	6.35 6.51	23.24	138.81

The synthetic dyke model (Figure 12) was assigned a susceptibility of 0.005981 SI. The number of data points (101), profile length (100m), thickness (2m), depth to top of anomaly (4m) and depth to bottom (8m). 5% and 10% random noise was added to the synthetic dataset and 2D analytic signal was computed from the noise corrupted synthetic anomalies using a frequency domain filtering undertaking as depicted by Agarwal and Srivastava (2008).

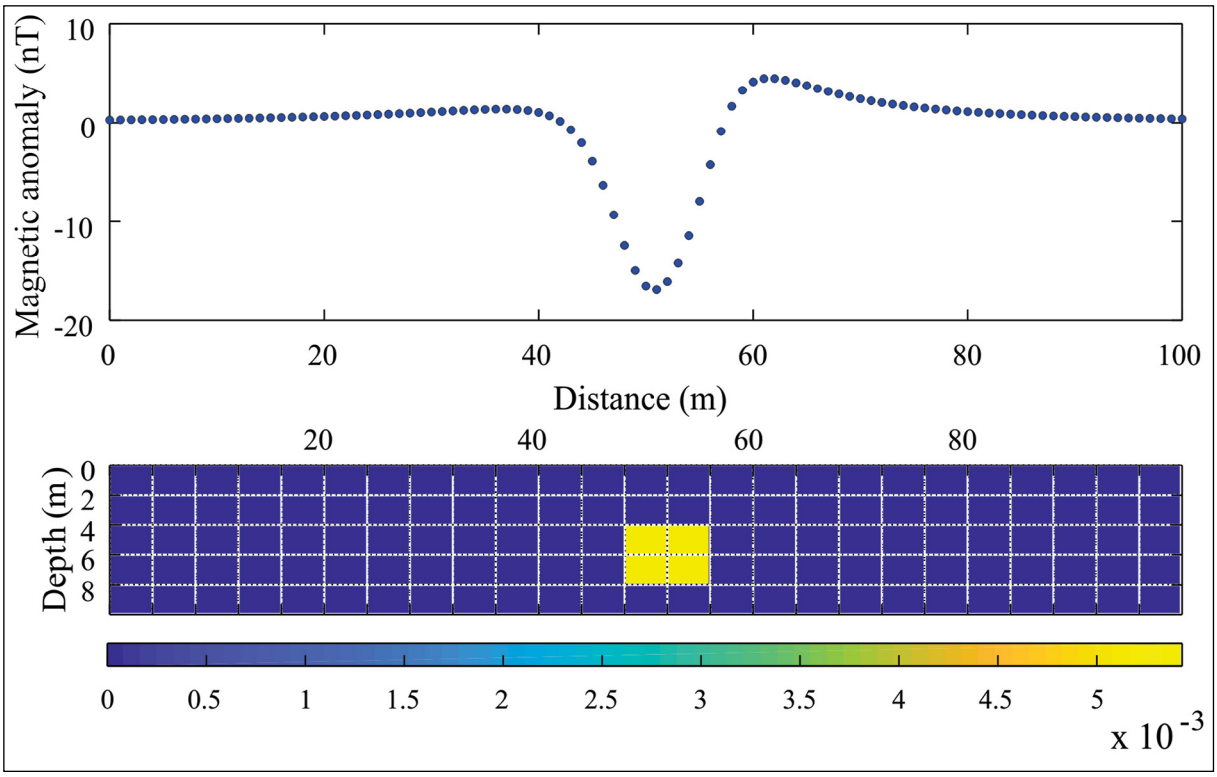

Figure 12- Synthetic anomaly with a dyke-like structure of 0.005982 magnetic susceptibility. Field intensity 33,000nT, inclination –10°.

The PSO program was tested with parameters from the synthetic data before application to the anomaly profiles taken from our study region. Figure 13 shows a plot of the initial computation (at 0% noise data) and Table 2 displays model parameters reckoned from PSO for the single dyke structure with various noise percentages and the r.m.s. error. The computed amplitude of analytic (AS) of the synthetic magnetic data is also shown on Figure 13. Model parameters were also computed with random noise addition of 5% and 10% successively.

We present the search spaces and computed/ interpreted model parameters from PSO for profiles *AA′, BB′ and CC′* on Tables 3, 4, and 5. Table 6 shows a comparison of interpreted model parameters from

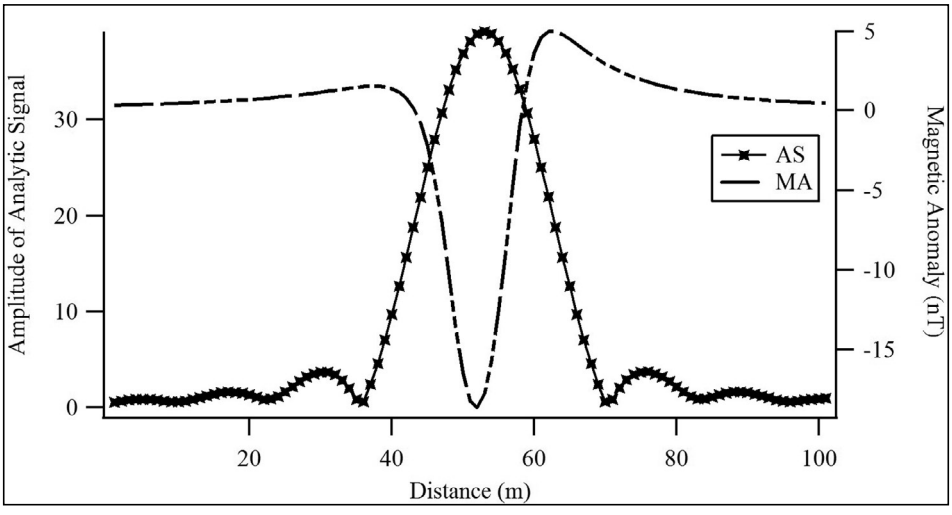

Figure 13- Synthetic Magnetic Anomaly data (0% noise) and its computed analytic signal.

Table 2- Model Parameters calculated from PSO for a single dyke with various noise percentages and their r.m.s. error. x_0 and z_0 are the coordinates of the source location in the unit of data spacing.

		Model space		Computed model parameters with random noise percentage		
	True model	Minimum	Maximum	0%	5%	10%
Amplitude	470	10	5000	490	515	520
x_0	55	10	100	56	56	58
z_0	4	1	12	4.5	4.5	4.8
q	1	0.2	1.5	1.0	1.0	0.9
	rms Error			0.03	0.24	1.05

Data spacing = 1m

Table 3- Search space for profile *AA′* taken across a mine site within the region of study with computed PSO parameters. x_0 and z_0 are the coordinates of the source location in the unit of data spacing.

	Model space		Computed parameters from PSO
	Minimum	Maximum	
Amplitude	10	3000	355
x_0	1	20	12.5
z_0	0.1	10	1.8
q	0.2	1.5	0.9
	r.m.s. error		0.1012

Data spacing = 0.5 km

Table 4- Search space for profile *BB′* taken across a mine site within the region of study with computed PSO parameters. x_0 and z_0 are the coordinate of the source location in the unit of data spacing.

	Model space		Computed parameters from PSO
	Minimum	Maximum	
Amplitude	10	5000	420
x_0	7	20	9
z_0	0.1	10	0.2
q	0.2	1.5	0.8
	r.m.s. error		0.0682

Data spacing = 0.5 km

Table 5- Search space for profile *CC′* taken across two notable sources and the computed PSO parameters. x_0 and z_0 are the coordinates of the source location in the unit of data spacing.

Bell 1				Bell 2		
	Model space		Computed parameters	Model space		Computed parameters
	Minimum	Maximum		Minimum	Maximum	
Amplitude	10	5000	590	10	5000	1120
x_0	2	10	6	10	30	16.1
z_0	0.1	10	0.4	0.1	10	0.29
q	0.2	1.5	0.9	0.2	1.5	0.88
	r.m.s. error		0.1663			0.1882

Data spacing = 0.5 km

ELW and PSO computations for the respective profiles under consideration.

A plot of magnetic anomalies (MA), amplitude of analytic signal (AS) from measured magnetic anomalies and amplitude of analytic signal calculated by utilizing interpreted model parameters from profiles *AA′, BB′ and CC′* is shown in Figures 14, 15 and 16.

4. Discussion

Tests on synthetic and field data (Pilkington, 2009) have shown that a more focused solution is produced from sparse inversion compared with a standard model – space, least-squares inversion. Our modeling results depicted in Figures 7 and 8 were realized from the modeling data of Figure 5. Figure 7 shows unit features embedded in the region. Various subsurface intrusions could be observed which contrasted with

Table 6- Interpreted model parameters from ELW and PSO modeling for profiles taken from the study region.

	Amplitude	Location (km)	Depth (km)	Structural Index
Profile AA'				
ELW	-	13.22	1.77	0.3
PSO	355	12.5	1.8	0.8
Profile BB'				
ELW	-	8.11	0.12	-0.35
PSO	420	9	0.2	0.8
Profile CC' (S1)				
ELW	-	5.28	0.38	0.85
PSO	590	6	0.4	0.9
Profile CC' (S2)				
ELW	-	15.34	0.27	1.02
PSO	1120	16.1	0.29	0.88

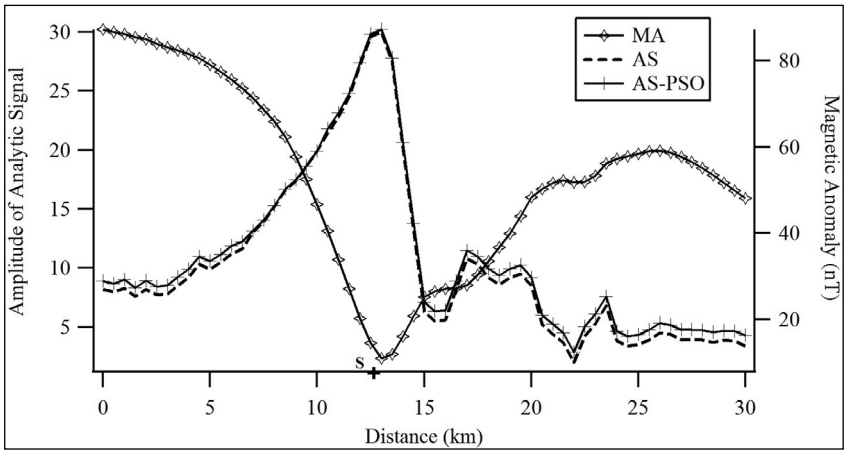

Figure 14- Magnetic anomaly (MA) over a source in profile *AA′* across the Enyigba mine site. AS, amplitude of 2D analytic signal from measured anomaly, AS-PSO, amplitude of analytic signal calculated by utilizing interpreted model parameters from PSO. The '+' sign indicate the horizontal position of the source.

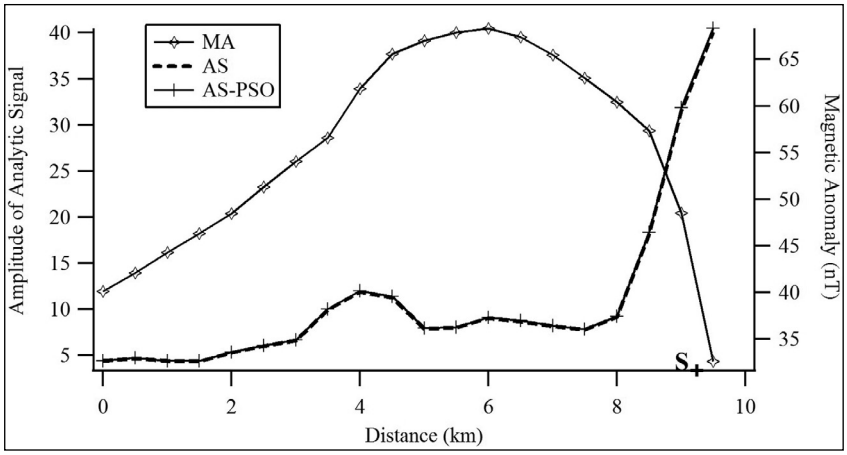

Figure 15- Magnetic anomaly (MA) over a source in profile *BB′* at Mkpuma-Ekwaokuko mine site. AS, amplitude of 2D analytic signal from measured anomaly, AS-PSO, amplitude of analytic signal calculated by utilizing interpreted model parameters from PSO. The '+' sign indicate the horizontal position of the source.

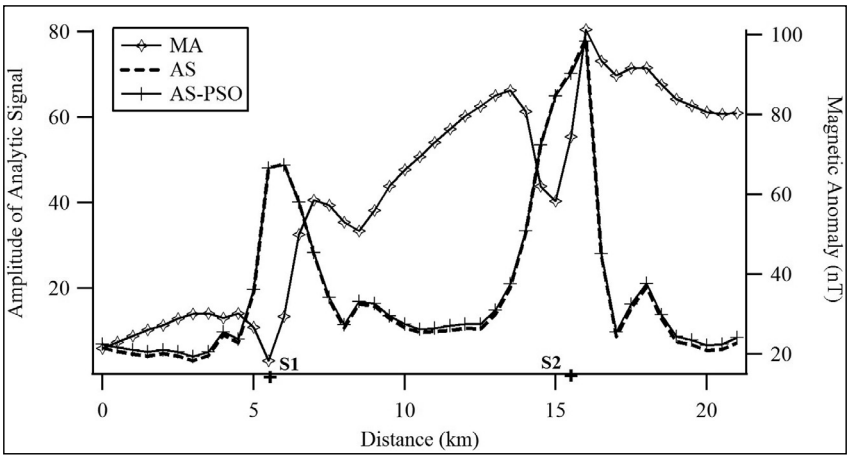

Figure 16- Magnetic anomaly (MA) over sources in profile *CC'*. AS, amplitude of 2D analytic signal from measured anomaly, AS-PSO, amplitude of analytic signal calculated by utilizing interpreted model parameters from PSO. The '+' sign indicates the horizontal position of the sources.

the background susceptibilities. We pegged the model susceptibility at 0.0005 *SI* due to the predominant background geology of the region (shale and sandstone with susceptibilities of 0.00065 and 0.0004 SI) (Dobrin and Savit, 1988; NGA, 2004) (Figure 7). We then clipped susceptibilities less than 0.00113 SI to bring out the contrasting bodies in the model.

Figure 8 displays various subsurface geologic features domiciled in the region. We interpret these features as geological units controlling mineralization in the region. To enable comparison and confirmation using the various locations of active mining activities in the region, we took a plan views of the modeled result (Figures 9 and 10). The model results capture most of the active mining locations in the region. The Enyigba mines location (Figure 9) indicates units with magnetic susceptibilities >0,00188 *SI* Some of the lower magnetic anomalies locates over high susceptibility units (as indicated within the drawn circles). The geometry of the resolved units (Figures 9) implies the union of magnetic anomaly with a metamorphic rock enveloped by the predominant shale formation in the region. The mining of rocks with lead-zinc (Pb-Zn) mineralization at Enyigba, ilmenite, and pyroclastic rocks at Abakaliki confirms this deduction. We also spotted an intrusion around Abba Omega that we identified as representing units bearing copper (Cu) or barite minerals (GSNA, 2004). Intrusions observed at Obubra are directly associated with traced volcanic rocks mapped as basalts, trachytes, and rhyolites (Figure 2) and that of the surrounding areas of Obubra (Eja and Ogurude localities) has an imposing record of lead (Pb) ore deposits. The inversion result at Ngbo – Ekerigwe area shows a significant magnetic body connected with intense remnant magnetization. The dimensions of the magnetic mass are almost 3.5 km in-depth extension and 18 km stretch in the northern E – W direction (Ngbo – Ekerigwe). This magnetic body has great prospectivity importance because of its structural and positional emplacement and could contribute to the metallogenic as well as structural comprehension of mineralization in the Asu River formation. Further integration with other geophysical data from the area could provide more information regarding the association of these magnetic bodies and yet to be discovered minerals in the region. Our modeling study has shown even more possible geological units hosting economically viable mineral resources yet recorded within the study region, showing subsurface extensions and their possible boundaries.

The Euler deconvolution map (Figure 10) shows derived source positions represented as circles and depth information proportional to their respective colour representations. We achieved good clustering of the solutions and they show definite magnetic trends aligning in the E–W, NW–SE, and NE–SW directions within the study region. The dominant linear features

trending NE – SW (FUNAI, Enyigba, Ishieke and Apiapum regions) and E – W (Abakaliki and Osebi regions) directions show many clustering and could be interpreted as faults within the study region. The NE – SW trend corresponds to the orientation of the trend produced by the Santonian deformation which affected the Lower Benue Trough (Ezema et al., 2014). Epigenetic fractures striking E-W, NW-SE, and N-S generally host mineralization (lead-zinc-baryte) in an area (Ford, 1981; Omada and Ike, 1996; Oha and Onuoha, 2013). We observed similar trends of anomalies over Abakaliki–Ugep regions as Anyanwu and Mamah outo2013) from their analysis of Landsat Thematic Mapper and airborne magnetic data. Magnetic edges – notable faults have been marked with good precision using a series of depth-labeled Euler trends (Pallero et al., 2015). The alignment of clusters from the 3D Euler solutions along the edges of contrasting magnetic intensities is also noted (Figure 10), with the structural contacts from Euler deconvolution aligning around the major solutions of the 3D model at the north-central region of the study area.

The analytic signal was evaluated to assess how well our modeling study matches the geological units in the region. We note that the model result agrees to some degree with obvious features realized from the analytic signal results (Figure 11). The AS assesses the amplitude of the gradient of magnetization; the closer we are to the magnetic sources, the higher the amplitude of that gradient. We observed that while the analytic signal computation was able to resolve the location of the present mines, the sparseness model could not resolve most of these anomalies. Nevertheless, the 3D model performed excellently in identifying deeper bodies (depths > 5000 m) with significant susceptibility contrast. Isolated and secluded maxima of the analytic signal results visible at the N-W, N-E and S-W regions of the study area were interpreted as stemming from subsurface intrusions at the respective locations. We observed matches of prominent anomaly features on the analytic signal map and the model solutions mainly with features located around the Ngbo, Ekerigwe, Mfuma, Obubra, and Onyen localities. The spread-out maximas notable at the S-E region could be due partly to some subsurface intrusions at the region, and also to the shallow crustal deposition of gravels, basalt and trachytes within the Eze Aku Shale formation of that region (Ovat, 2015). Obande et al. (2014) adopted a similar interpretation approach in their study area with similar magnetization properties. We recall that Figure 2 showed the basaltic and rhyolitic intrusions at Obubra which may also influence the magnetic anomaly record for the region.

Analysis of the AS by PSO technique (Tables 3, 4 and 5) indicates that the structural index of the anomaly source identified from processing Profile AA' data (Figures 11 and 14) suggests the presence of an intruded dyke structure within the region. The index value from ELW computation (0.3) may also hint on a closed interaction of contact sources with the dyke structure at this location. This contact source interaction is clearly seen on the overlain magnetic anomaly data with the Euler and 3D model solutions (Figure 10). NE – SW trending geologic contact sources are mapped around the Enyigba – FUNAI region, sandwiching the Enyigba mine fields and also following the mapped out isolated region by the analytic signal results as seen in Figure 10. The present Pb-Zn mineral mining operations in the area is noted to extend vertically downwards in the open cast mining pits at this location and may confirm our dyke structure interpretation of the anomaly from this location. The extension of these anomalies within and around the Enyigba mine field (Figure 10) may also suggest capturing the edges of a sill structure around the region. Profile BB' was considered given the presence of the Mkpuma-Ekwaokuko mine field (ME) (Figures 5 and 11) and a notable maximum from the analytic signal at that location. This site is currently being exploited for Pb-Zn minerals by the locals. Examinations of the magnetic anomalies indicate similar magnetic features with the Enyigba mine field location. However, the limited data at the time of this study restricted the extent of our profile, therefore we located our profile from the center of the examined anomaly outwards (Figure 11). Table 4 shows model search space and computed parameters from PSO for profile BB'. A r.m.s. error of 0.0682 was also achieved from the computations. PSO computed a depth of 0.2 km at horizontal distance of 9.0 km for the location. Figure 15 shows a plot of the magnetic

anomaly over the source in profile *BB*′. Computations using the ELW technique presented a depth of 0.12 km at a horizontal distance of 8.11 km. The structural indices from the ELW and PSO techniques (Table 6) reveals an interaction of contact sources with the dyke structure within the subsurface at that location. The AS computed from Profile *CC*′ data exhibits two peaks of significantly different amplitudes (Figures 11 and 16). In the absence of drill hole information at this location, the AS computation has clearly revealed the presence of the two distinct sources along this profile. Our inversion of the AS involved fitting two bells corresponding to the two peaks observed. Table 5 presents the model parameter search spaces and the realized computed parameters from PSO for both bells (Profile *CC*′). The r.m.s. error is also shown. The peaks analyzed in these results may indicate causative sources located at S1 and S2 to be vertical dyke structures separated by approximately 3 km. The structural indices from the ELW and PSO computations (Table 6) confirm that the causative sources are vertical dyke structures intruded at the location.

5. Conclusion

We have performed a 3D magnetic inversion modeling of geologic units representing mineralization structures in Abakaliki and environs. The 3D inversion results aligned with the analytic signal solution calculated from the same anomaly data. This region in the southeastern zone of Nigeria is known to host vast mineral deposits of economic significance. Good clustering of the Euler deconvolution solutions were obtained for the region and revealed definite magnetic trends aligning in the E–W, NW–SE, and NE–SW directions. The dominant linear features trending NE – SW around the Enyigba mine fields have been noted to play an active role in the mineralization of the region. The contact sources interact with the dyke structure identified in the region using analytic signal technique and a global optimization technique (PSO). In general, PSO results are comparable to those achieved by the ELW technique and indicate stability of solutions and reliability of results. Several other subsurface geologic units which possibly represent mineralization structures in the region have been recognized. Inversion of both magnetic anomaly and analytical signal has enabled derivation of the actual subsurface structures in the region with most of the structures appearing as dykes with depths ranging from 0.2 – 1.8 km at most of the mining sites in the region. Structural indices computed for the region have also indicated interaction of contact sources (faults and fractures) with identified dyke structures. This study has confirmed most of the sites currently being excavated for these minerals and also show potential sites whose locations were hitherto unknown which could also be considered for further exploration. Results have contributed to the knowledge base of geologic units representative of the mineralization structures in southeastern Nigeria. Quantitative analysis provided by this study would enable informed geotechnical engineering decisions especially at potential mining sites.

Acknowledgments

We are grateful to the anonymous reviewers, including the editor, whose comments contributed to improve this manuscript. We also acknowledge Dr. Ben Earl Barrowes of Engineer Research and Development Center – U.S. Army for his advice on the programs. Dr. Harish Garg of Thapar Institute of Engineering and Technology, Patiala, School of Mathematics, is also recognized for his advice on the PSO program. This research did not receive any specific grant from funding agencies in the public, commercial, or not-for-profit sectors.We would like to declare that total compliance with ethical standards was observed in the preparation of this manuscript and the submitted manuscript posses no conflict of interest between the authors and any other party.

References

Abdelrahman, E. M., El-Araby, H. M., El-Araby, T. M., Essa, K. S. 2003. A least-squares minimization approach to depth determination from magnetic data: Pure and Applied Geophysics 160, 1259–1271.

Aboud, E., Wameyo, P., Alqahtani, F., Moufti, M. R. 2018. Imaging subsurface northern Rahat Volcanic Field, Madinah city, Saudi Arabia, using Magnetotelluric study. Journal of Applied Geophysics 159, 564 – 572.

Abraham, E. M., Alile, O. M. 2019. Modelling Subsurface Geologic Structures at Ikogosi Geothermal Field,

Southwestern Nigeria, using Gravity, Magnetics, and Seismic Interferometry Techniques. Journal of Geophysics and Engineering 16, 729– 741.

Abraham, E. M., Itumoh, O., Chukwu, C., Rock, O. 2018. Geothermal Energy Reconnaissance of Southeastern Nigeria from Analysis of Aeromagnetic and Gravity-Data. Pure and Applied Geophysics, 176, 22 – 36.

Agarwal, B. N. P., Srivastava, S. 2008. FORTRAN codes to implement enhanced-local-wave-number technique to determine location, depth and shape of the causative source using magnetic anomaly. Computer Geosciences 34, 1843–1849.

Agha, S. O., Arua, A. I. 2014. Integrated-geophysical investigation of sequence of deposition of sedimentary strata in Abakaliki, Nigeria. European Journal of Physical and Agricultural Sciences 2(1) 1-5.

Anyanwu, G., Mamah, L. 2013. Structural Interpretation of Abakaliki-Ugep using Airborne magnetic and Landsat Thematic Mapper (TM) data. Journal of Natural Science Research 3(13) 20-31

Benkhelil, J. 1988. Structure Et Evolution Geodynamique De basis Intercontinental De Ca Benoue (Nigeria). Bulletin des Centres de Researches Exploration – Production ELF Aquaintaine 1207, 29.

Büyüksaraç, A., Reiprich, S., Ates¸ A. 1998. Three-dimensional magnetic model of amphibolite complex in Taskesti area, Mudurnu valley, North-West Turkey. Journal Of The Balkan Geophysical Society 1 (3) 44-52.

Büyüksaraç, A., Jordanova, D., Ates¸ A., Karloukovski, V. 2005. Interpretation of the Gravity and Magnetic Anomalies of the Cappadocia Region, Central Turkey. Pure Applied Geophysics 162, 2197–2213.

Clerc, M. 1999. The swarm and the queen: towards a deterministic and adaptive, particle swarm optimization. The Proceedings of International Conference on Evolutionary Computing, Washington 1951–1957.

Couto, M. A., Aisengart, T., Barbosa, D., Ferreira, R. C. R., Baltazar, O. F., Marinho, M., Cavalcanti, A. D., Araujo, J. C. S. 2017. Magnetization-Vector Inversion, Application in quadrilatero Ferrifero region, MG, Brazil. 15th International Congress of the Brazil Geophysical Society, Rio de Janeiro, Brazil.

Dobrin, M. B., Savit, C. H. 1988. Introduction to geophysical prospecting. McGraw-Hill Book Co. 867.

Eshaghzadeh, A., Seyedi Sahebari, S., Dehghanpour, A. 2020. 3D inverse modeling of the gravity field due to a chromite deposit using the Marquardt's algorithm and forced neural network. Bulletin of the Mineral Research and Exploration 161, 33-47.

Essa, K. S., Munschy, M. 2019. Gravity data interpretation using the particle swarm optimization method with application to mineral exploration. Journal of Earth System Science 128, 123.

Essa, K. S., Elhussein, M. 2020. Interpretation of magnetic data through particle swarm optimization: Mineral exploration cases studies. Natural Resources Research 29, 521–537.

Essa, K. S., Abo-Ezz, E. R. 2021. Potential field data interpretation to detect the parameters of buried geometries by applying a nonlinear least-squares approach. Acta Geodaetica et Geophysica 56, 387 – 406.

Essa, K. S., Nady, A. G., Mostafa, M. S., Elhussein, M. 2018. Implementation of potential field data to depict the structural lineaments of the Sinai Peninsula, Egypt. Journal of African Earth Sciences 147, 43–53.

Essa, K. S., Mehanee, S., Elhussein, M. 2021. Magnetic Data Profiles Interpretation for Mineralized Buried Structures Identification Applying the Variance Analysis Method. Pure and Applied Geophysics 178, 973–993.

Eze, L. C., Mamah, L. I. 1985. Electromagnetic, and Ground Magnetic survey, over zones of Lead-Zinc Mineralization in Wanakom (Cross River State). Journal of Earth sciences 7, 749.

Ezema, P. O., Doris, E. I., Ugwu, G. Z., Abdullahi, U. A. 2014. Hydrocarbon and mineral exploration in Abakaliki, southeastern-Nigeria. The International Journal of Engineering and Science 3(1), 24-30.

Ford, S. O. 1981. The Economic Mineral Resources of the Benue-Trough. Earth Evolution Sciences 2, 154-163.

Ganguli, S. S., Singh, S., Das, N., Maurya, D., Pal, S. K., Rama Rao, J. V. 2019. Gravity and magnetic survey in south western part of Cuddapah Basin, India and its implication for shallow crustal architecture and mineralization. Journal of Geological Society of India 93(4) 419-430.

Ganguli, S. S., Pal, S. K., Kumar, S. K. P. 2021. Insights into the crustal architecture from the analysis of gravity and magnetic data across Salem-Attur Shear Zone (SASZ), Southern Granulite Terrane (SGT), India: an evidence of accretional tectonics. Episodes 44(4) 419 – 422.

GSNA, 2004. Mineral resources map of Nigeria. Geological-Survey of Nigeria Agency(GSNA).

Huang, L., Guan, Z. 1998. Discussion on Magnetic-interpretation using the 3-D analytic signal,

by Walter R. Roest, Jacob Verhoef, and Mark Pilkingtonç Geophysics 63, 667–670.

Jain, S. 1988. Total magnetic field reduction—The Pole or Equator? A model study. Canadian Journal of Exploration Geophysics 24 (2) 185–192

Kennedy, J., Eberhart, R. 1995. Particle-swarm optimization. The Proceedings of IEEE Conference on Neural Networks, Piscataway, NJ 1942–1948.

Kowalczyk, P., Oldenburg, D., Phillips, N., Nguyen, T. H., Thomson, V. 2010. Acquisition and analysis of the 2007–2009 geosciences BC-airborne data. The Australian, SEG-PESA Airborne, Gravity Workshop.

Kumar, S., Pal, S. K., Guha, A., Sahoo, S. D., Mukherjee, A. 2020. New insights on Kimberlite emplacement around the Bundelkhand Craton using integrated satellite-based remote sensing, gravity, and magnetic data. Geocarto International 37 (4) 999 – 1021.

Leâo-Santos, M., Li, Y., Moraes, R. 2015. Application of 3D-magnetic amplitude inversion, to iron oxide-copper-gold deposits, at low magnetic latitudes: A case-study from Carajas Mineral Province, Brazil. Geophysics 80(2) B13 – B22.

Lelievre, P. G. 2003. Forward modeling and inversion of geophysical magnetic data. A master's thesis submitted to The University of British Columbia.

Leu, L. K. 1981. Use of reduction-to-the-equator process for magnetic data interpretation. Geophysics 47, 445.

Li, X. 2003. On the use of different methods for estimating magnetic depth. Leading Edge 22, 1090–1099.

Li, Y., Sun, J. 2016. Geology-differentiation with uncertainty estimation using inverted-magnetization directions. SEG International Exposition and 86th Annual Meeting 2159

MacLeod, I. N., Ellis, R. G. 2013. Magnetic vector inversion a simple approach to the challenge of varying direction of rock magnetization. ASEG-PESA 2013. 23rd International Geophysical Conference and Exhibition, 11-14 August 2013-Melbourne, Australia.

Mahmoodi, O., Smith, R. S., Spicer, B. 2016. Using constrained, inversion of gravity and magnetic-field to produce a 3D litho-prediction model. SEG Inter. Exposition and 86th Annual Meeting 2170 – 2174.

Mehanee, S., Essa, K. S., Diab, Z. E. 2021. Magnetic data interpretation using a new R-parameter imaging method with application to mineral exploration: Natural Resources Research 30, 77–95.

Melo, A. T., Sun, J., Li, Y. 2015. Geophysical-inversions applied to geological differentiation, and deposit characterization: A case study at an IOCG deposit in Carajás-Mineral-Province, Brazil. 85th Annual International Meeting, SEG, Expanded Abstracts 2012–2016.

Nabighian, M. N. 1972. The analytic signal of two-dimensional magnetic bodies with polygonal cross-section: its properties and use for automated anomaly interpretation. Geophysics 37, 507–517

NGA, 2004. GM-SYS Gravity/Magnetic Modeling Software. Northwest Geophysical Associates, Inc., USA.

Nwachukwu, S. O. 1972. The Tectonic Evolution of the Southern Portion of the Benue Trough, Nigeria. Geological Magazine 109, 411-419.

Obande, G. E., Lawal, K. M., Ahmed, L. A. 2014. Spectral analysis of aeromagnetic data for geothermal investigation of Wikki Warm Spring, north-east Nigeria. Geothermics 50, 85–90.

Obarezi, J. E., Nwosu, J. I. 2013. Structural Controls, of Pb-Zn Mineralization, of Enyigba District, Abakaliki, Southeastern Nigeria. Journal of Geology and Mining Research 5 (11) 250-261.

Ofoegbu, C. O. 1985. A review of the Geology of the Benue Trough. Nigeria, Journal of African Earth Science 3, 283.

Oha, I. A., Onuoha, K. M. 2013. Contrasting Styles of Pb-Zn-Ba Mineralization in the Lower Benue Trough, Southern Nigeria. A paper presented at the 49th Annual International Conference and Exhibitions of the Nigerian Mining and Geosciences Society (NMGS), Ibadan, March 2013.

Olade, M. A. 1975. Evolution of Nigeria's Benue-Trough (Aulacogen): A tectonic model. Geological Magazine 112, 575–581.

Omada, J. I., Ike, E. C. 1996. On the Economic Appraisal and Genesis of the Barite Mineralization and Saline Springs in the Middle-Benue-Trough. Nigeria. Journal of Mineralogy, Petrology and Economic Geology 91,109-115

Ovat, O. O. 2015. Obubra yesterday, today, and tomorrow: An assessment of the economic development of a local government area in Cross River State. Nigeria. Journal of Economic and Sustainable Developments 6 (20) 78 – 86.

Pallero, J. L. G., Fernandez-Martinez, J. L., Bonvalot, S., Fudym, O. 2015. Gravity inversion and uncertainty assessment of basement relief via Particle Swarm Optimization. Journal of Applied Geophysics 116,180–191.

Pilkington, M. 2009. 3D magnetic data-space inversion with sparseness constraints. Geophysics 74 (1) P.L7-L15.

Pilkington, M., Bardossy, Z. 2015. DSIM3D: software to perform unconstrained-3D-inversion of magnetic data. Geological Survey of Canada.

Press, W. H., Teukolsky, S. A., Vetterling, W. T., Flannery, B. P. 1994. Numerical Recipes in FORTRAN. Cambridge University Press, New Delhi.

Reid, A. B., Thurston, J. B. 2014. The structural index in gravity and magnetic interpretation: Errors, uses, and abuses. Geophysics 79, J61-J66.

Reid, A. B., Allsop, J. M., Grauser, H., Millet, A. J., Somerton, I. N. 1990. Magnetic interpretation in 3D using Euler-Deconvolution. Geophysics 55, 80-91

Riedel, S. 2008. Airborne-Based geophysical investigation in Dronning Maud land Antarctica. Dissertation, Christian Albrechts Universitat Zu Kiel, Kiel.

Roest, W. R., Verhoef, J., Pilkington, M. 1992. Magnetic interpretation using the 3D analytic signal. Geophysics 57 (1) 116-125.

Sacchi, M. D., Ulrych, T. J. 1995. High-resolution velocity gathers and offset space reconstruction: Geophysics 60, 1169–1177.

Salem, A., Ravat, D., Smith, R. S., Ushijima, K. 2005. Interpretation of magnetic data using an enhanced local wave number (ELW) method. Geophysics 70, L7–L12.

Srivardhan, V., Pal, S. K., Vaish, J., Kumar, S., Bharti, A. K., Priyam, P. 2016. Particle swarm optimization inversion of self -potential data for depth estimation of coal ¦res over East Basuria colliery, Jharia coal field, India. Environmental Earth Sciences 75(8) 1-12.

Srivastava, S., Agarwal, B. N. P. 2010. Inversion of the amplitude of the two-dimensional analytic signal of the magnetic anomaly by the particle swarm optimization technique. Geophysical Journal International 182, 652-662.

Srivastava, S., Pal, S. K., Rajwardhan, K. 2020. A time-lapse study using Self-Potential and Electrical Resistivity Tomography methods for mapping of old mine working across railway-tracks in a part of Raniganj Coalfield, India. Environmental Earth Sciences 79, 332.

Stocco, S., Godio, A., Sambuelli, L. 2009. Modelling and compact inversion of magnetic data: A Matlab code. Computers and Geosciences 35, 2111–2118

Thompson, D. T. 1982. Euldph: A new technique, for making computer-assisted, depth- estimates, from magnetic data, Geophysics 47, 31-37

Thurston, J. B., Smith, R. S. 1997. Automatic conversion of magnetic data to depth, dip, and susceptibility contrast using the SPITM method. Geophysics 62, 807–813.

Ugwu, G. Z., Alasi, T. K. 2016. Aeromagnetic Survey for Determining Depth, to Magnetic Source of Abakaliki and Ugep Areas, of the Lower Benue Trough, Nigeria. Engineering and Technology Journal 1(1) 18 – 31.

Whitehead, N., Musselman, C. 2005. Montaj Gravity/ Magnetic interpretation: Processing, analysis, and visualization system, for 3-D inversion of potential field data, for Oasis montaj v6.1. Geosoft Inc. ON, Canada.

Yao, C. 2007. Iterative 3-D gravity and magnetic inversion for physical properties. SEG/San Antonio 2007 Annual meeting 805 – 810.